Observable tensor-to-scalar ratio and secondary gravitational wave background

Arindam Chatterjee[1] and Anupam Mazumdar[2,3]

[1]Indian Statistical Institute, 203, B.T. Road, Kolkata 700108, India
[2]Van Swinderen Institute, University of Groningen, 9747 AG Groningen, The Netherlands
[3]Kapteyn Astronomical Institute, University of Groningen, 9700 AV Groningen, The Netherlands

(Received 7 September 2017; published 19 March 2018)

In this paper we will highlight how a simple vacuum energy dominated *inflection-point* inflation can match the current data from cosmic microwave background radiation, and predict large primordial tensor to scalar ratio, $r \sim \mathcal{O}(10^{-3} - 10^{-2})$, with observable second order gravitational wave background, which can be *potentially* detectable from future experiments, such as DECi-hertz Interferometer Gravitational wave Observatory (DECIGO), Laser Interferometer Space Antenna (eLISA), cosmic explorer (CE), and big bang observatory (BBO).

DOI: 10.1103/PhysRevD.97.063517

I. INTRODUCTION

Detecting the primordial gravitational waves (GWs) will lead to the finest imprints of the nascent Universe, which will confirm the inflationary paradigm [1], quantum nature of gravity [2,3], and a new scale of physics beyond the standard model (BSM). During the slow roll inflation one can excite both scalar and tensor perturbations, see [4], and the interesting observable parameter is the tensor-to-scalar ratio, r. There are many models of inflation, see [5], which can predict both large and small r, while matching the other observables, such as the amplitude of temperature anisotropy, the tilt in the power spectrum, and its running of the spectrum by the cosmic microwave background radiation (CMBR) [6], within the observed window of $\mathcal{O}(8)$ e-foldings of primordial inflation from the Planck satellite. However, it is worthwhile also to constrain the potential beyond the *pivot scale*, $k_* = 0.05\ \mathrm{Mpc}^{-1}$, where the relevant observables are normalised.

The aim of this paper will be to provide a simple toy model example of inflationary potential, which can generate large tensor perturbations, in particular large *potentially observable*, r, by the ground based experiments such as BICEP-Keck array [7], and also leave imprints of GWs with a frequency range, $10^{-4} - 10^{3}$ Hz, at DECi-hertz Interferometer Gravitational wave Observatory (DECIGO) [8], Laser Interferometer Space Antenna (eLISA) [9], cosmic explorer (CE) [10], and big bang observer (BBO) [11], see also [12]. Therefore, correlating GWs at two different frequencies and wavelengths *inspired* by the same model of inflation.

II. THE POTENTIAL, TENSOR-TO-SCALAR RATIO AND BENCHMARK POINTS

As we will show, *inflection-point* models of inflation [13,14], provides this unique possibility to excite the GWs from the *pivot scale*, where the CMBR observables are normalized to the end of inflation.

In order to illustrate this, let us now consider a simple potential which allows *inflection-point*, and we will *strictly* assume that $\phi_{\rm CMB}, \Delta\phi_{\rm CMB} \leq M_p$ [14–16].

$$V(\phi) = V_0 + A\phi^2 - B\phi^n + C\phi^{2(n-1)}, \tag{1}$$

where V_0 corresponds to cosmological constant term during inflation, the coefficients A, B, C are appropriate constants with dimensions, and $n \geq 3$ is an integer. The physical motivation for the above potential *directly* comes from a softly broken supersymmetric theory with a renormalizable and nonrenormalizable superpotential contribution with canonical Kähler potential, see [13]. In these papers it was assumed that $V_0 = 0$. However, the supergravity extension, naturally provides cosmological constant, V_0 if no fine tuning is invoked to cancel such a contribution, see for details [14]. Inflation will have to come to an end via phase transition, or via hybrid mechanism [17]. In the present work we will also explore the possibility of having large V_0, in particular to achieve potentially observable $r \geq \mathcal{O}(10^{-3})$ at the pivot scale.

In the above Eq. (1), V_0, A, B, C are all subject to various cosmological constraints from the latest Planck data [6], here we quote the central values, which we will use for the reconstruction of V_0, A, B, C from the following *well-known* observables:

$$A_{\rm s} \approx \frac{V}{24\pi^2 M_{\rm pl}^4 \varepsilon_V} \approx 2.2 \times 10^{-9} \tag{2}$$

$$n_{\rm s} \approx 1 + 2\eta_V - 6\varepsilon_V \approx 0.96 \tag{3}$$

TABLE I. We have used $n_s = 0.96, A_s = 2.2 \times 10^{-9}, \phi_{\rm CMB} = 1$ in the Planck units for all the benchmarks evaluated at $k_* = 0.05$ Mpc^{-1}. The three benchmark points match the current CMBR data, i.e. the central values used in Eqs. (2), (3).

Benchmark Points (BP)	n	$V_0(k_*)$	$A(k_*)$	$B(k_*)$	$C(k_*)$	$\frac{dn_s}{d\ln k}(k_*)$	$\frac{d^2n_s}{d\ln k^2}(k_*)$	$r(k_*)$
1	3	7.44×10^{-10}	0.868×10^{-10}	0.689×10^{-10}	0.190×10^{-10}	−0.006	0.003	0.024
2	3	1.506×10^{-10}	0.2046×10^{-10}	0.2246×10^{-10}	0.0757×10^{-10}	−0.0148	0.001	0.005
3	4	14.245×10^{-10}	1.240×10^{-10}	0.500×10^{-10}	0.112×10^{-10}	−0.0148	0.021	0.046

$$\mathrm{d}n_s/\mathrm{d}\ln k \approx 16\varepsilon_V\eta_V - 24\varepsilon_V^2 - 2\xi_V^2 \approx -0.013 \quad (4)$$

$$\mathrm{d}^2n_s/\mathrm{d}\ln k^2 \approx -192\varepsilon_V^3 + 192\varepsilon_V^2\eta_V - 32\varepsilon_V\eta_V^2 - 24\varepsilon_V\xi_V^2 + 2\eta_V\xi_V^2 + 2\sigma_V^3 \approx 0.03, \quad (5)$$

where $\varepsilon_V, \eta_V, \xi_V, \sigma_V$ are slow-roll parameters defined below. All the above quantities are measured at the *pivot* scale, $k_* = 0.05$ Mpc^{-1}, and we have considered the central values in this paper, such as A_s is the amplitude of the scalar power spectrum, $n_s(k_*)$ is the spectral tilt, $\mathrm{d}n_s/\mathrm{d}\ln k(k_*)$ is the running of the tilt and $\mathrm{d}^2n_s/\mathrm{d}\ln k^2(k_*)$ designates the running of the running of the tilt [6]. Further note that the slow roll parameters can be expressed in terms of the potential, and given by, see review [5]:

$$\varepsilon_V = \frac{M_P^2}{2}\left(\frac{V'}{V}\right)^2; \qquad \eta_V = M_P^2\left(\frac{V''}{V}\right); \quad (6)$$

$$\xi_V^2 = M_P^4\left(\frac{V'V'''}{V^2}\right); \qquad \sigma_V^3 = M_P^6\left(\frac{V'^2V''''}{V^3}\right). \quad (7)$$

Another *key* formula is the tensor perturbations and the value of r, and its tilt, which are given by:

$$A_{\rm t} \approx \frac{2V}{3\pi^2M_{\rm pl}^4}, \qquad r(k=k_*) = \frac{\mathrm{A}_t}{\mathrm{A}_s}. \quad n_{\rm t} \approx -2\varepsilon_V, \quad (8)$$

In fact, the coefficients, A, B, C can be computed in terms of $V_0, \mathrm{A}_s, r, n_s$, with the help of the following relation, see [15,16].[1]:

$$V(\phi_{\rm CMB}) = \frac{3}{2}A_sr\pi^2, \qquad V'(\phi_{\rm CMB}) = \frac{3}{2}\sqrt{\frac{r}{8}}(A_sr\pi^2),$$
$$V''(\phi_{\rm CMB}) = \frac{3}{4}\left(\frac{3r}{8} + n_s - 1\right)(A_sr\pi^2). \quad (9)$$

Given the observable constraints, see Eqs. (2), (3), (4), (5) we scan the parameter space by fixing the value of $n = 3, 4$. By insisting that the total number of e-foldings of inflation to be $\mathcal{N} = 50$ along with $\phi_{\rm CMB} \sim \mathcal{O}(M_p)$, we obtain the following benchmark points, as tabulated in Table. I.

Note that, as discussed in Refs. [15,16], with $\phi_{\rm CMB} = 1$, assuming specific r and varying V_0 the parameters A, B, C have been reconstructed using the data. Further, choice of large V_0 implies that there is no significant fine-tuning among the relevant parameters involved [18]. Further, for a specific choice of r, a small range of V_0 (and the other parameters) can remain viable after considering additional constraints from $\mathrm{d}n_s/\mathrm{d}\ln k, \mathrm{d}^2n_s/\mathrm{d}\ln k^2$.

We have numerically solved the Mukhanov-Sasaki equation [19] without using the slow-roll approximations to obtain the scalar power spectrum P_s for the three benchmark points, see [I], two of them are for renormalizable potentials, and one for nonrenormalizable potential. These have been shown in Fig. 1. We illustrate the power spectrum beyond the Planck window of $\mathcal{O}(8)$ e-foldings, and show that the scalar amplitude grows outside this observable window, and reaches $P_s(k) \leq 10^{-1.5}$ for $k \leq 10^{20}$ Mpc^{-1} at the end of 50 e-foldings of inflation. This happens due to the fact that both ϵ_V, η_V change nonmonotonically within the observational window of $\mathcal{O}(8)$ e-foldings. At the *pivot* point, $k = 0.05$ Mpc^{-1}, the scalar power spectrum, the tilt and its running all match the observed data, see Table I, and Eqs. (2), (3), (4), (5), but after the inflaton has crossed $\phi_{\rm CMB}$, or the *pivot* point, the value of ϵ_V reaches its maximum, and then decreases rapidly, while the other slow roll parameter η_V decrease before increasing again as ϕ decreases [15,16].

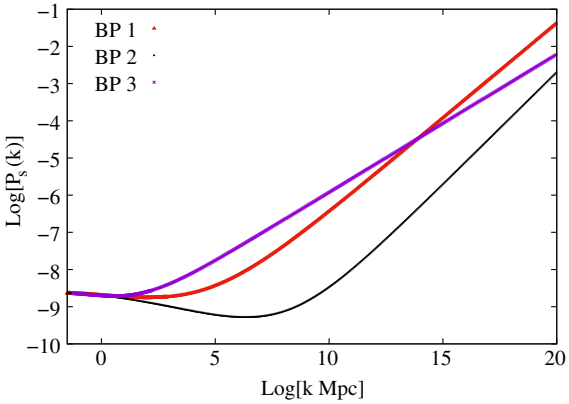

FIG. 1. The scalar power spectra has been shown for the benchmark scenarios in Table I.

[1]As will be shown in Fig. 2, the slow-roll parameters are small enough at the pivot scale, and therefore the reconstruction in Eq. (9) holds good at the pivot scale.

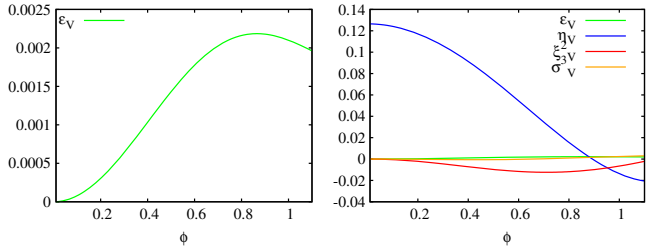

FIG. 2. The slow-roll parameters have been shown for the benchmark scenario BP-3 in Table I.

The evolution of the slow-roll parameters have been shown in Fig. 2 for BP-3 in order to demonstrate these features. As shown in the figure, the slow-roll parameters are small enough around the pivot scale $\phi_{\rm CMB} = 1$ to ensure the validity of the parameter reconstruction. As the slow-roll parameters, especially η_V becomes large as the inflation proceeds, we numerically solve the full Mukhanov-Sasaki equation [19] to obtain the scalar power spectrum, as discussed above.

At small $\phi \ll \phi_{\rm CMB}$, the slow roll parameter $\eta_V \to \frac{2A}{V_0}$. As shown in Fig. 2, it is the large η_V at small $\phi \ll \phi_{\rm CMB}$, that leads to more power at small length scales. This property was first noticed in [15]. Note that, for large V_0, it can dominate the energy density well after the CMB observable window to the end of the inflation, inflation will typically end via phase transition as discussed above. In our case, there is be a bumplike feature in the potential close to the pivot scale. This, in turn, gives rise to large r corresponding to the benchmark points.

Here we briefly comment on the importance of the parameters we have chosen. With $\phi_{\rm CMB} = 1$, using Eq. (9), it is possible reconstruct the potential with less number of parameters, e.g., V_0, A, B for a particular choice of r. However, we have found that for $n = 3$, for $\epsilon_V \lesssim \mathcal{O}(10^{-3})$, $B > 0$; this makes the potential unbounded from below. Also, the running of n_s, which we compute after reconstructing the potential parameters using A_s, n_s for a specific choice of r, can impose further constraint on the viability of the reconstructed parameters. A further reduction of the number of parameters (with $\phi_{\rm CMB} = 1$) would make it impossible to reconstruct for a given r, since the number of parameters involved would be less than that of the equations.

In this paper we will not discuss how to end inflation, and how to reheat the Universe in any detail [20], but we will now discuss the possibility of generating GWs at different length scales and frequencies.

Now, since the scalar power spectrum has an increasing trend in the infrared, see Fig. 1, one can ask whether this would source any gravitational waves at the second order. The gravitational perturbations can be sourced by the matter perturbations at the second order, this has been studied in Refs. [21,22]. Based on this we can ask how much the amplification of GWs will be at scales around $\mathcal{O}(10^{10} - 10^{20})$ Mpc^{-1}? Also, what will be the frequency range of these GWs, and would they be detectable by DECIGO, eLISA, CE, and BBO?

III. SECONDARY OBSERVABLE GRAVITATIONAL WAVES

In order to understand this amplification of the GWs, let us first study the metric perturbations, defined as,

$$ds^2 = -a(\eta)^2\Big[(1+2\Phi)d\eta^2 + \Big\{(1-2\Phi)\delta_{ij} + \frac{1}{2}h_{ij}\Big\}dx^i dx^j\Big]$$

where Φ is the metric potential, we have taken anisotropic stress to be absent, and h_{ij} denotes the second-order tensor perturbation, which satisfies $h^i_i = 0, h^j_{i,j} = 0$ (i.e. traceless and transverse conditions). We are keen on the tensor perturbations, which can be expressed as follows,

$$h_{ij}(\mathbf{x},\eta) = \frac{1}{(2\pi)^{3/2}}\int d^3\mathbf{k}\, e^{i\mathbf{k}.\mathbf{x}}[h_{\mathbf{k}}(\eta)e_{ij}(\mathbf{k}) + \bar{h}_{\mathbf{k}}(\eta)\tilde{e}_{ij}(\mathbf{k})]$$

The two polarization tensors in the above equations are normalized, such that $e^{ij}e_{ij} = 1 = \tilde{e}^{ij}\tilde{e}_{ij}, e^{ij}\tilde{e}_{ij} = 0$.

Note that, at *large* k ($k \gtrsim 10^8$ Mpc^{-1}) *of our interest*, the first-order tensor perturbation during inflation is negligible. To compute the power spectrum, and then the corresponding energy density, it is convenient to work in Fourier space. By expanding the Einstein tensor and the energy-momentum tensor up to the second-order, and substituting the same in the Einstein equation, the following equation can be obtained [21,22],[2]

$$h''_{\mathbf{k}} + 2\mathcal{H}h'_{\mathbf{k}} + k^2 h_{\mathbf{k}} = \mathcal{S}(\mathbf{k},\eta). \tag{10}$$

The source term $\mathcal{S}(\mathbf{k},\eta)$ can be written as [21,22],

$$\mathcal{S}(\mathbf{k},\eta) = -4e^{lm}(\mathbf{k})\mathcal{S}_{lm}(\mathbf{k}) = \int \frac{d^3\mathbf{q}}{(2\pi)^{3/2}} e^{lm}(\mathbf{k})q_l q_m \mathcal{F}(\mathbf{k},\mathbf{q},\eta), \tag{11}$$

where,

[2]While the Eq. (10) holds for the "+" polarization $e_{ij}(\mathbf{k})$, the amplitude $\bar{h}_{\mathbf{k}}$, corresponding to the "×" polarization also obeys a similar equation. Note that we follow the normalization in [21,22] for the polarization tensors. Several references follow a different convention, see, e.g., Ref [23].

$$\mathcal{F}(\mathbf{k},\mathbf{q},\eta) = 12\Phi(q,\eta)\Phi(|\mathbf{k}-\mathbf{q}|,\eta) + \frac{8}{\mathcal{H}}\Phi'(q,\eta)\Phi(|\mathbf{k}-\mathbf{q}|,\eta) + \frac{4}{\mathcal{H}^2}\Phi'(q,\eta)\Phi'(|\mathbf{k}-\mathbf{q}|,\eta). \quad (12)$$

To estimate the source term, we evaluate the Bardeen potential first [4]. Since the scalar power spectrum starts rising for $k \gg k_{\rm eq} \sim 0.01$ Mpc^{-1}, the second-order source term can only be significant for $k \gg k_{\rm eq}$. Consequently, we only consider the modes which are reentering the Hubble patch during the radiation domination. In this epoch, the Bardeen potential satisfies the following evolution equation:

$$\Phi'' + \frac{6(1+w)}{(1+3w)\eta}\Phi' + wk^2\Phi = 0, \quad (13)$$

with $w = 1/3$. Ignoring the decaying mode at early times, the solution takes the following form:

$$\Phi(k,\eta) = \frac{c(k)}{(k\eta)^3}\left[\frac{k\eta}{\sqrt{3}}\cos\left(\frac{k\eta}{\sqrt{3}}\right) - \sin\left(\frac{k\eta}{\sqrt{3}}\right)\right]. \quad (14)$$

Note that the Bardeen potential $\Phi(k)$ can be split in to two parts, a contribution from the primordial perturbation $\phi_{\mathbf{k}}$ ($\eta \ll 1$) and the transfer function as $\Phi(k,\eta) = \Phi(k\eta)\phi_{\mathbf{k}}$. The coefficient $c(k)$ is estimated matching of $\Phi(k,\eta)$ with the primordial perturbation at $\eta \ll 1$. This gives $\Phi(k,\eta \ll 1) = -c(k)/9\sqrt{3}$. Thus $c(k)$ can be estimated from the primordial power spectrum as follows [21],

$$c(k)^2 \simeq (9\sqrt{3})^2\frac{4}{9}\frac{2\pi^2}{k^3}P_s(k) = \frac{216\pi^2}{k^3}P_s(k) \quad (15)$$

where $P_s(k)$ denote the primordial scalar power spectrum (i.e. the power spectrum as $\eta \to 0$). Before getting into the numerical results, we describe the behavior of the amplitude $h_{\mathbf{k}}$ and the source term first [22]. The amplitude $h_{\mathbf{k}}$ is largest at a time η_i, when $k\eta_i \simeq 1$, i.e., during the period of Hubble reentry of the respective mode. At this point its amplitude can be simply estimated as $S(\mathbf{k},\eta_i)/k^2$. Once a mode enters horizon, it starts oscillating, and the amplitude decreases as inverse of the scale factor. Also, the source term $S(\mathbf{k})$ decreases faster during radiation domination before eventually becoming constant during matter dominated epoch. For our benchmarks, see Table I, we find that the source term scales as $1/a^{\gamma}$, where $\gamma \simeq 2$–3. For the modes, which enter early in the radiation dominated epoch, the source term can become too small before entering the matter dominated epoch, so the amplitude simply decreases as inverse of the scale factor until today. The energy density of the gravitational wave (in logarithmic intervals of k) is given by (see, e.g., [23]),

$$\rho_{\rm GW}(k,\eta) = \frac{\langle \dot{h}_{ij}\dot{h}^{ij}\rangle}{32\pi G} = \frac{1}{32\pi G}\frac{k^2}{a(\eta)^2}\mathcal{P}_h(k,\eta), \quad (16)$$

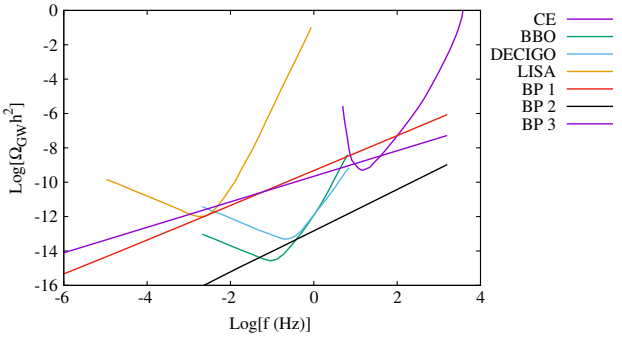

FIG. 3. The relative contribution of the gravitational wave to the energy density has been shown for the benchmark scenarios in Table I.

where η is the conformal time, and the power spectrum $\mathcal{P}_h(k,\eta)$ takes the following form

$$\mathcal{P}_h(k,\eta) = \frac{k^3}{2\pi^2}(|h_{\mathbf{k}}(\eta)|^2 + |\bar{h}_{\mathbf{k}}(\eta)|^2). \quad (17)$$

The relative energy density $\Omega_{\rm GW}(k,\eta) = (1/12)(k^2/a(\eta)^2H(\eta)^2)\mathcal{P}_h(k,\eta)$, then, can be estimated at the present epoch by, $(\Omega^0_{\rm rad}h^2/\Omega^{\rm eq}_{\rm rad})\Omega^{\rm eq}_{\rm GW}(k)$, where we take $h = 0.68$, and $\Omega^{\rm eq}_{\rm GW}(k)$ evaluated at the reentry

$$\Omega^0_{\rm GW}(k)h^2 = \frac{\Omega^0_{\rm rad}h^2}{2\Omega^{\rm eq}_{\rm rad}}\left(\frac{g_{*\rm eq}}{g_{*i}}\right)^{1/3}\frac{k^2\mathcal{P}_h(k,\eta_i)}{12a(\eta_i)^2H(\eta_i)^2}. \quad (18)$$

where η_i represents the conformal time around the Hubble reentry of the respective mode when the amplitude $h_{\mathbf{k}}$ is maximum, thus $k\eta_i \sim \mathcal{O}(1)$. During radiation domination $\rho_{\rm total} = \rho_{\rm rad} \propto H(\eta)^2 \propto g_*^{-1/3}a^{-4}$. Further, the effective number of degree of freedom contributing to the energy density and to the entropy density have been assumed to be the same during this epoch, with $g_{*\rm eq} = 106.75$, $g_* = 3.36$ and $\Omega_{\rm rad}h^2 \simeq 4.3 \times 10^{-5}$. We show the estimated $\Omega^0_{\rm GW}(k)h^2$ for the benchmark scenarios in Fig. 3. Note that the BBN and CMBR constraints on $\Omega_{\rm GW}$ (i.e., $\Omega_{\rm GW} \lesssim 10^{-5}$, see, e.g., [24]) is satisfied by our benchmark scenarios.

IV. DISCUSSION AND CONCLUSION

Since the scalar power spectrum, as depicted in Fig. 1 for our benchmark scenarios, rises only after $k \sim 10^4$ Mpc^{-1}, these remain unaffected by future constraints from COBE/FIRAS on CMB y and μ distortions; in future PIXIE may be able to impose moderate constraints in some cases [25,26]. Furthermore, large scalar perturbation at small scales can possibly lead to enhanced structure formation at smaller scales[3] We have used available constraints on small

[3]The large scale structure (LSS) and Ly-α data is relevant on scales of $\sim\mathcal{O}(10)$ Mpc^{-1}. To our knowledge no numerical simulation for large scale structure uses resolution smaller than pc. We could not find any constraints on the scalar power spectrum at very small scales relevant for us in the literature.

scale compact objects, most notably primordial blackholes (PBHs), to ensure the viability of our benchmark scenarios. Since the scalar power spectra only become large well after matter radiation equality, we have estimated PBH formation during radiation domination epoch for these benchmark scenarios. The mass of a PBH formed during the horizon-entry of a scale k (during radiation dominated epoch) can be estimated as,

$$M_{\rm PBH}(k) = 2.48 \times 10^{46} \frac{\gamma}{k^2}\ {\rm g}. \tag{19}$$

where γ denotes the energy fraction within the horizon which ends up inside the PBH. It depends on the details of the gravitational collapse, and have been estimated to be approximately $(1/3)^{3/2} \simeq 0.2$ during the radiation dominated epoch [27–29]. Thus, large scalar power at large k, as is relevant for our benchmarks, corresponds to a small PBH mass, i.e. $\ll \mathcal{O}(10^{10})$ gm. We have used Press-Schechter formalism [30], while assuming spherical collapse, with the threshold density contrast $\delta_{\rm th} = \frac{1}{3}$, and a Gaussian window function to estimate the PBH formation [27,28]. Also, the Gaussian distribution has been assumed for smoothening the density perturbations.[4] We have found that for all our benchmarks the most abundant PBH masses are well below $\mathcal{O}(10^{10})$ gm, and these typically contribute much less than 10^{-20} to the fraction of the energy density in the respective epoch. Therefore, there is no stringent constraint from photo-dissociation or hadron injection during BBN [25,28].

Before concluding, let us point out to the key physics for generating large primordial r. This is due to the presence of V_0 term. It is conceivable that instead of V_0, one might be able to invoke many scalar fields giving rise to an enhancement in the Hubble expansion rate [35]. It would be interesting to see if multi-scalar fields can also reproduce sufficiently blue tilt in the power spectrum beyond the 8 e-foldings of observed window via *inflection-point* inflation.

To summarize, we have provided an example of inflationary potential, which is capable of generating large tensor-to-scalar ratio, in our scans we have given examples of $r = 0.024, 0.046, 0.005$. These values of r are generated by the *inflection-point* inflation, which provides large running of the slow roll parameters outside the *pivot* scale such that the power spectrum increases in the infrared until the end of inflation. The latter sources the secondary GWs with $\Omega_{\rm GW}h^2 \leq 10^{-6}$, which can be potentially detectable by DECIGO, eLISA, BBO, and CE, therefore, opening up new vistas for GW cosmology.

[4]Generally the mass of the PBHs formed and the relevant parameters can depend on the details of the nature of the collapse, see, e.g., [31–34]. We have not considered such effects. For simplicity, we have also assumed that PBHs of mass $M_{\rm PBH}(k)$ are only formed during the hubble entry of a scale k, and have not considered"critical phenomenon" [31], and PBH merger.

ACKNOWLEDGMENTS

A. C. acknowledges financial support from the Department of Science and Technology, Government of India through the INSPIRE Faculty Award /2016/DST/INSPIRE/04/2015/000110.

[1] A. H. Guth, The inflationary universe: A possible solution to the horizon and flatness problems, Phys. Rev. D **23**, 347 (1981); A. A. Starobinsky, A new type of isotropic cosmological models without singularity, Phys. Lett. **91B**, 99 (1980); A. D. Linde, A new inflationary universe scenario: A possible solution of the horizon, flatness, homogeneity, isotropy and primordial monopole problems, Phys. Lett. **108B**, 389 (1982); A. Albrecht and P. J. Steinhardt, Cosmology for Grand Unified Theories with Radiatively Induced Symmetry Breaking, Phys. Rev. Lett. **48**, 1220 (1982).

[2] L. P. Grishchuk, Amplification of gravitational waves in an istropic universe, Zh. Eksp. Teor. Fiz. **67**, 825 (1974) [Sov. Phys. JETP **40**, 409 (1975)].

[3] A. Ashoorioon, P. S. Bhupal Dev, and A. Mazumdar, Implications of purely classical gravity for inflationary tensor modes, Mod. Phys. Lett. A **29**, 1450163 (2014).

[4] J. M. Bardeen, Gauge invariant cosmological perturbations, Phys. Rev. D **22**, 1882 (1980); J. M. Bardeen, P. J. Steinhardt, and M. S. Turner, Spontaneous creation of almost scale-free density perturbations in an inflationary universe, Phys. Rev. D **28**, 679 (1983); H. Kodama and M. Sasaki, Cosmological perturbation theory, Prog. Theor. Phys. Suppl. **78**, 1 (1984).

[5] A. Mazumdar and J. Rocher, Particle physics models of inflation and curvaton scenarios, Phys. Rep. **497**, 85 (2011).

[6] P. A. R. Ade *et al.* (Planck Collaboration), Planck 2015 results. XIII. Cosmological parameters, Astron. Astrophys. **594**, A13 (2016).

[7] P. A. R. Ade *et al.* (BICEP2 and Planck Collaborations), Joint Analysis of BICEP2/Keck Array and Planck Data, Phys. Rev. Lett. **114**, 101301 (2015).

[8] S. Kawamura *et al.*, The Japanese space gravitational wave antenna: DECIGO, Classical Quantum Gravity **28**, 094011 (2011).

[9] P. Amaro-Seoane *et al.*, eLISA/NGO: Astrophysics and cosmology in the gravitational-wave millihertz regime, GW Notes **6**, 4 (2013).

[10] B. P. Abbott *et al.* (LIGO Scientific Collaboration), Exploring the sensitivity of next generation gravitational wave detectors, Classical Quantum Gravity **34**, 044001 (2017).
[11] E. S. Phinney *et al.*, The Big Bang Observer: Direct detection of gravitational waves from the birth of the Universe to the Present, *NASA Mission Concept Study* (2004).
[12] C. J. Moore, R. H. Cole, and C. P. L. Berry, Gravitational-wave sensitivity curves, Classical Quantum Gravity **32**, 015014 (2015).
[13] R. Allahverdi, K. Enqvist, J. Garcia-Bellido, and A. Mazumdar, Gauge Invariant MSSM Inflaton, Phys. Rev. Lett. **97**, 191304 (2006); R. Allahverdi, K. Enqvist, J. Garcia-Bellido, A. Jokinen, and A. Mazumdar, MSSM flat direction inflation: Slow roll, stability, fine tunning and reheating, J. Cosmol. Astropart. Phys. 06 (2007) 019; R. Allahverdi, A. Kusenko, and A. Mazumdar, A-term inflation and the smallness of neutrino masses, J. Cosmol. Astropart. Phys. 07 (2007) 018; A. Chatterjee and A. Mazumdar, Tuned MSSM Higgses as an inflaton, J. Cosmol. Astropart. Phys. 09 (2011) 009.
[14] A. Mazumdar, S. Nadathur, and P. Stephens, Inflation with large supergravity corrections, Phys. Rev. D **85**, 045001 (2012).
[15] S. Hotchkiss, A. Mazumdar, and S. Nadathur, Observable gravitational waves from inflation with small field excursions, J. Cosmol. Astropart. Phys. 02 (2012) 008.
[16] A. Chatterjee and A. Mazumdar, Bound on largest $r \lesssim 0.1$ from sub-Planckian excursions of inflaton, J. Cosmol. Astropart. Phys. 01 (2015) 031.
[17] A. D. Linde, Axions in inflationary cosmology, Phys. Lett. B **259**, 38 (1991); Hybrid inflation, Phys. Rev. D **49**, 748 (1994).
[18] S. Hotchkiss, A. Mazumdar, and S. Nadathur, Inflection point inflation: WMAP constraints and a solution to the fine tuning problem, J. Cosmol. Astropart. Phys. 06 (2011) 002.
[19] V. F. Mukhanov, Quantum theory of gauge invariant cosmological perturbations, Zh. Eksp. Teor. Fiz. **94N7**, 1 (1988) [Sov. Phys. JETP **67**, 1297 (1988)]; M. Sasaki, Gauge invariant scalar perturbations in the new inflationary universe, Prog. Theor. Phys. **70**, 394 (1983).
[20] R. Allahverdi, R. Brandenberger, F. Y. Cyr-Racine, and A. Mazumdar, Reheating in inflationary cosmology: Theory and applications, Annu. Rev. Nucl. Part. Sci. **60**, 27 (2010).
[21] K. N. Ananda, C. Clarkson, and D. Wands, The cosmological gravitational wave background from primordial density perturbations, Phys. Rev. D **75**, 123518 (2007).
[22] D. Baumann, P. J. Steinhardt, K. Takahashi, and K. Ichiki, Gravitational wave spectrum induced by primordial scalar perturbations, Phys. Rev. D **76**, 084019 (2007).
[23] M. Maggiore, Gravitational wave experiments and early universe cosmology, Phys. Rep. **331**, 283 (2000).
[24] T. L. Smith, E. Pierpaoli, and M. Kamionkowski, A New Cosmic Microwave Background Constraint to Primordial Gravitational Waves, Phys. Rev. Lett. **97**, 021301 (2006); H. Assadullahi and D. Wands, Constraints on primordial density perturbations from induced gravitational waves, Phys. Rev. D **81**, 023527 (2010).
[25] A. S. Josan, A. M. Green, and K. A. Malik, Generalised constraints on the curvature perturbation from primordial black holes, Phys. Rev. D **79**, 103520 (2009); R. Emami and G. Smoot, Observational constraints on the primordial curvature power spectrum, J. Cosmol. Astropart. Phys. 01 (2018) 007.
[26] J. Chluba, A. L. Erickcek, and I. Ben-Dayan, Probing the inflaton: Small-scale power spectrum constraints from measurements of the CMB energy spectrum, Astrophys. J. **758**, 76 (2012).
[27] B. J. Carr, The primordial black hole mass spectrum, Astrophys. J. **201**, 1 (1975); B. J. Carr, J. H. Gilbert, and J. E. Lidsey, Black hole relics and inflation: Limits on blue perturbation spectra, Phys. Rev. D **50**, 4853 (1994).
[28] B. J. Carr, K. Kohri, Y. Sendouda, and J. Yokoyama, New cosmological constraints on primordial black holes, Phys. Rev. D **81**, 104019 (2010).
[29] B. Carr, F. Kuhnel, and M. Sandstad, Primordial black holes as dark matter, Phys. Rev. D **94**, 083504 (2016).
[30] W. H. Press and P. Schechter, Formation of galaxies and clusters of galaxies by self-similar gravitational condensation, Astrophys. J. **187**, 425 (1974).
[31] J. C. Niemeyer and K. Jedamzik, Near-Critical Gravitational Collapse and the Initial Mass Function of Primordial Black Holes, Phys. Rev. Lett. **80**, 5481 (1998).
[32] J. C. Hidalgo and A. G. Polnarev, Probability of primordial black hole formation and its dependence on the radial profile of initial configurations, Phys. Rev. D **79**, 044006 (2009).
[33] I. Musco, J. C. Miller, and L. Rezzolla, Computations of primordial black hole formation, Classical Quantum Gravity **22**, 1405 (2005).
[34] I. Musco, J. C. Miller, and A. G. Polnarev, Primordial black hole formation in the radiative era: Investigation of the critical nature of the collapse, Classical Quantum Gravity **26**, 235001 (2009).
[35] A. R. Liddle, A. Mazumdar, and F. E. Schunck, Assisted inflation, Phys. Rev. D **58**, 061301 (1998).